J Math Chem (2014) 52:2395–2410
DOI 10.1007/s10910-014-0377-2

ORIGINAL PAPER

Constructing quantum mechanical models from diabatic schemes: external field modulation of effective energy barriers for bond breaking/formation processes

Gustavo A. Arteca · Laura Laverdure · O. Tapia

Received: 30 April 2014 / Accepted: 14 June 2014 / Published online: 22 July 2014

Abstract We have recently proposed an approach where chemical transformations can be described as quantum processes involving the modulation of entangled states by an applied external field (Arteca and Tapia in Phys Rev A 84:012115, 2011). In practical implementations, we gain insight into these processes by using simple quantum-mechanical models derived from diabatic schemes. In this context, reactant, product, and, eventually, intermediate species, are assigned to diabatic basis functions, and then entangled by an external field into a quantum state from which all observable properties of the chemical reaction should emerge. Here, we extend our previous model for bond breaking/formation in diatomic molecules (Arteca et al. in J Math Chem 50:949, 2012). We consider the entire manifold of semiclassical models defined by only two diabatic basis functions: a harmonic well for the "molecular" bound state, and an exponential potential energy function for the asymptotically separated fragments (the "product" channel). Using a two-parameter space to describe all models, we determine how the topology of the total energy function is affected by the shape of the applied field. We show that strong and weak local couplings with the external field modify substantially the occurrence of energy barriers, in contrast to using the uniform (i.e., space-invariant) coupling employed in previous works.

Keywords Separable models · Nonisolated systems · Semiclassical potentials · Diabatic states

G. A. Arteca (✉) · L. Laverdure
Département de Chimie et Biochimie and Biomolecular Sciences Programme, Laurentian University, Ramsey Lake Road, Sudbury, ON P3E 2C6, Canada
e-mail: gustavo@laurentian.ca

G. A. Arteca · O. Tapia
Department of Physical and Analytical Chemistry, Uppsala University, Ångström Building, Box 259, 751 05 Uppsala, Sweden

1 Introduction

The role of external fields on the modulation of chemical processes is central for understanding their fundamental mechanisms, as well as developing technologically relevant applications. An electric or radiation field affects not only the energetics and the rate of a given reaction, but it can also modify its mechanism [1], including the possible opening of reactions pathways that are forbidden under conventional thermal or photochemical conditions [2,3]. In addition, external-field modulation can be used to change the nature of molecular states, for instance, by making them more confined [4–8]. The ability to control "molecular trapping" has enormous potential for encoding quantum information using nanotechnology [9–11].

In this work, we deal with conceptually simple models for chemical processes that incorporate all the above characteristics [12,13]. Using the elementary process of breaking (or forming) a single chemical bond, we analyze the ability of the external field to alter the topology of the total-energy function. In particular, we study how the intensity and the spatial shape of the applied field pulse modifies, and eventually suppresses, the occurrence of reaction barriers to bond breaking/formation.

Our approach views all chemical transformations as electronic (i.e., fully quantum) transitions. In this methodology, chemical processes emerge from the properties of entangled states [12–15]. These states can be seen as linear (coherent) superpositions allowed (and modulated) by the external field; for simplicity and convenience, we adopt a diabatic scheme for their representation [14–16]. The practical implementation, referred to as the generalized electronic diabatic (GED) protocol, uses a set of *diabatic basis functions* to represent the superposition states for the nonisolated system (refs. [12–17], others therein). Conceptually, these functions can be viewed as representing the quantum states for the "isolated chemical species", i.e., when the external field is absent. The number of components in the coherent superposition is dictated by the symmetry of the problem, as well as the number of reaction channels of interest. In turn, these are dictated by the energy window opened by the intensity, shape, and duration of the applied field pulse. Here, we deal with a minimalistic model that involves the coupling of *only two* diabatic electronic basis functions.

The advantages of the GED methodology are twofold:

(a) By their diabatic nature, the isolated chemical species are strictly *single attractors*, that is, they are electronic functions that are independent from the nuclear configurations. Each of these basis functions is associated with a single potential energy minimum, i.e., cannot lead to a different species unless entangled with an applied field [12–16].
(b) The qualitative behaviours emerging from a GED-scheme for chemical processes depends mainly on the *shape* of the diabatic attractors. As a result, we can often bypass the construction of the diabatic basis set, and derive qualitative trends by using simple models of semiclassical potential energy attractors [12,13].

In this work, we profit from these two properties to discuss the role of the external field. To this end, we consider a two-state model of bond breaking/formation, corresponding to a coherent superposition of a molecular "reactant state," and an asymptotically separated fragmental "product state." This simple model can describe

a process whose symmetry does not require the incorporation of a third intermediate state (e.g., a diabatic "transition state") [12,18,19]. When using a weak electric field, we find such a process if both reactant and product channels are open-shell configurations, e.g., when breaking a diatomic radical bond: $(AB)^{\cdot} \rightarrow A^{\cdot} + B$ (cf. the breaking the H_2^+ molecule studied in ref. [13]).

Until now, we have focused on the role of the field intensity to modify the topology of the total-energy function [12,13] or reaction-path geometry [18,19] in two- and three-state models. In these analyses, we have used both semiclassical models [20–22], or actual quantum electronic basis functions [12,13], to illustrate the use of diabatic schemes.

In this work, we extend these ideas to a *manifold* of models. By using a two-parameter space, we determine the "phase" diagram of energy topologies by finding the models that either lead to the occurrence or absence of reaction barriers. The two chosen parameters are: (*i*) the vibrational frequency of the harmonic well for "molecular reactant," and (*ii*) the energy "pseudo-barrier" associated with the diabatic crossing, i.e., the "apparent" energy barrier in absence of applied field. These two parameters merely identify the particular model; in absence of an external field, *no* process is possible and therefore there is no "reaction barrier." The actual barrier emerges from the entanglement of reactant and product states by the external mediator.

The work is organized as follows: in the next section, we briefly describe the model and the type of external-field couplings considered. The next section describes how weak and strong local couplings affect the "phase diagram" for semiclassical models. We analyze how both the shape and intensity of the field changes the topology of the energy function, and we contrast our findings with that of the uniform (configurationally featureless) external-field coupling used in our previous works [13]. We close with a summary of conclusions and possible implications of our results regarding the construction of chemical reaction models within diabatic schemes.

2 Two-state semiclassical model for a quantum state entangled with the external field

2.1 General formalism

The basic ideas behind our model have been described elsewhere [12–15]. We summarize here the main extensions needed to analyze the effects of the external field shape.

Let us consider a general electronic Hamiltonian, $\hat{H}_e(\hat{\mathbf{q}}, \boldsymbol{\xi})$, defined with respect to the $\{\mathbf{q}\}$-space of electronic coordinates (with $\mathbf{q} = (\mathbf{q}_1, \ldots, \mathbf{q}_n)$, for n electrons), and an array of classical (massless) test charges at $\{\boldsymbol{\xi}\}$-positions (with $\boldsymbol{\xi} = (\boldsymbol{\xi}_1, \ldots, \boldsymbol{\xi}_N)$, for N nuclei):

$$\hat{H}_e(\hat{\mathbf{q}}, \boldsymbol{\xi}) = \hat{T}_e(\hat{\mathbf{q}}) + V_{ee}(\hat{\mathbf{q}}, \hat{\mathbf{q}}') + V_{Ne}(\hat{\mathbf{q}}, \boldsymbol{\xi}), \tag{1}$$

where $\hat{T}_e$, V_{ee}, and V_{Ne} are, respectively, the electronic kinetic operator and potential energy operators for the interelectronic repulsion and nuclear-electronic attraction.

In this context, the set of $\{\boldsymbol{\xi}_i\}$-coordinates can be seen as an externally controlled array of background charges which, together with any other applied field, can be used to probe the responses of the quantum system. Note that the $\{\boldsymbol{\xi}\}$-coordinates are in laboratory space, while the $\{\mathbf{q}_i\}$-parameters sustain the abstract Hilbert space of electronic eigenfunctions.

In our case, quantum states are represented as linear superpositions in a basis set of *diabatic* functions $\{\psi_s(\mathbf{q})\}$. These functions are solutions of the Hamiltonian (1) at *particular* $\{\boldsymbol{\xi}^{(k)}\}$-configurations [14],

$$\hat{H}_e(\hat{\mathbf{q}}, \boldsymbol{\xi}^{(k)})\psi_s(\mathbf{q}) = E_s(\boldsymbol{\xi}^{(k)})\,\psi_s(\mathbf{q}). \tag{2}$$

Each solution in Eq. (2) gives rise to a *diabatic potential energy attractor*:

$$\langle\psi_k(\hat{\mathbf{q}})|\hat{H}_e(\hat{\mathbf{q}}, \boldsymbol{\xi})\psi_k(\hat{\mathbf{q}})\rangle_{\mathbf{q}} = U_k(\boldsymbol{\xi}), \tag{3}$$

where the single minimum of each $U_k(\boldsymbol{\xi})$-attractor coincides with the kth eigenvalue in Eq. (2), $E_k(\boldsymbol{\xi}^{(k)}) = U_k(\boldsymbol{\xi}^{(k)}) = \min U_k(\boldsymbol{\xi})$. (The notation $\langle|\rangle_{\mathbf{q}}$ indicates integration over the $\mathbf{q}$-coordinates).

Each semiclassical $U_k(\boldsymbol{\xi})$-potential energy function (and its corresponding $\psi_k(\mathbf{q})$-basis function) describes an *isolated* system, i.e., the diabatic solution where *no* reaction is possible. Below, we study the properties of the *nonisolated* system by modeling the $U_k(\boldsymbol{\xi})$-potentials, rather than the $\psi_k(\mathbf{q})$-functions. This approach is convenient and expedient when seeking only qualitative trends in behaviour over a manifold of possible models. In contrast, the analysis of a particular chemical system requires the specific construction of the $\{\psi_k\}$-diabatic solutions, as explained in refs. [12] and [13].

The application of an external field modifies the kinetic energy operator $\hat{T}_e$ in Eq. (1) by adding a contribution from the vector potential, $\mathbf{A}$, to the linear momentum operator for the electrons, $\hat{\mathbf{p}}$ [14]. In the case of applying a quasi-static radiation field (and neglecting the high-field $||\mathbf{A}||^2$ contribution), the $\hat{H}_e$-operator is enlarged to produce the classical/quantum operators for the nonisolated molecular system, denoted by $\hat{H}_{full}$:

$$\hat{H}_{full} = \hat{H}_e(\hat{\mathbf{q}}, \boldsymbol{\xi}) + \hat{V}_{field}, \quad \text{with} \quad \hat{V}_{field} \approx -(e/mc)\mathbf{A}\cdot\hat{\mathbf{p}} \tag{4}$$

where $\hat{V}_{field}$ shares the parity of the electronic $\hat{\mathbf{p}}$-operator. Depending on the particular system or setup, $\mathbf{A}$ can have different symmetries in laboratory $\boldsymbol{\xi}$-space. In previous works, we have considered only $\hat{V}_{field}$-operators that are $\boldsymbol{\xi}$-independent, i.e., defined by spatially uniform external $\mathbf{A}$-fields where only their intensities were variable [12,13]. In this work, we contrast these previous results with those emerging from external fields with geometry profiles that are relevant to actual experimental setups (e.g., lorentzian shaped pulses in $\boldsymbol{\xi}$-space) [7,8].

The quantum states for the system dressed in the $\mathbf{A}$-field are denoted by $|\Phi(\mathbf{q}; \boldsymbol{\xi}, \mathbf{A})\rangle$, where q is the actual variable while $\boldsymbol{\xi}$ and $\mathbf{A}$ are "external" parameters. These states produce a total potential energy function $E_{full}(\boldsymbol{\xi})$ (also a function of $\mathbf{A}$): □

$$E_{full}(\boldsymbol{\xi}) = \langle \Phi(\mathbf{q}; \boldsymbol{\xi}, \mathbf{A}) | \hat{H}_{full}\, \Phi(\mathbf{q}; \boldsymbol{\xi}, \mathbf{A}) \rangle_{\mathbf{q}}. \tag{5}$$

In our representation, the $\{\Phi\}$-functions are described as linear superpositions in the basis set of electronic diabatic functions emerging from the eigenvalue Eq. (2):

$$\Phi(\mathbf{q}, \boldsymbol{\xi}, \mathbf{A}) = \sum_k C_k(\boldsymbol{\xi}, \mathrm{A}) \psi_k(\mathbf{q}). \tag{6}$$

The linear $\{C_k\}$-coefficients depend on all external parameters, namely, the $\{\boldsymbol{\xi}_i\}$-distribution of classical charges and the **A**-radiation field. The function in Eq. (6) represents an entangled state between those of the isolated system, the latter being modeled in our case by the $\{|\psi_k\rangle\}$-solutions. We can now proceed to study the properties of the E_{full}-function (Eq. 5) in terms of $\boldsymbol{\xi}$ and **A** by using only semiclassical representations for the $\{U_k(\boldsymbol{\xi})\}$-attractors.

2.2 Manifold of two-state models for bond breaking/formation

In order to illustrate qualitative trends in the bond breaking of diatomic radicals, we deal with two generic semiclassical diabatic potential energy functions, U_1 and U_2. In this context, the U_1 function is associated with the molecular bound state, while U_2 is associated with the asymptotic dissociation channel. In order to compare with previous models [21,22], we adopt a harmonic U_1 potential and an exponential repulsive state U_2:

$$U_1(x) = \frac{k}{2} x^2, \tag{7a}$$

$$U_2(x) = s\, e^{-x} + t, \tag{7b}$$

where the laboratory coordinate x is a relative deviation in internuclear separation, and it plays the role of the $\boldsymbol{\xi}$-coordinates in Eq. (3). All quantities in Eq. (7) are dimensionless.

We have considered the manifold defined over a range of k and t values, while keeping the pre-exponential parameter $s = 1$. As a physically appealing parameter space, we use a pair of variables $(k^{1/2}, \Delta)$, where $k^{1/2}$ is the dimensionless harmonic frequency and Δ is the "diabatic pseudo-barrier height," i.e., the energy at the diabatic crossing $U_1(x_+) = U_2(x_+)$, relative to the asymptotic energy value for $x \to +\infty$:

$$\Delta = U_1(x_+) - t. \tag{8}$$

In the present context, Δ is employed merely as a useful parameter to characterize the model; in absence of external field, Δ is *not* associated with any actual physical barrier. For each (k, t)-pair, the Δ-value is computed numerically from the transcendental equation $U_1(x_+) = U_2(x_+)$. (We omit the second solution $x_- < 0$ for the high-energy diabatic crossing associated with bond contractions). The resulting $\Delta(k)$-function satisfies the following limiting behaviours for $s = 1$:

$$\Delta \approx 1 - \left(\frac{2(t+1)}{k}\right)^{1/2} + \frac{2+t}{k}, \quad \text{for all } t \text{ and } k \geq 6, \tag{9a}$$

$$\Delta \approx e^{-\sqrt{(2t/k)}}, \quad \text{for large } t \text{ and small } k \text{ values.} \tag{9b}$$

Each possible model appears as a $(k^{1/2}, \Delta)$-point, approximately bound between the curves in Eq. (9). Using this approach, we have analyzed the curvature properties of the E_{full}-function in $(k^{1/2}, \Delta)$-parameter space for $k^{1/2} \leq 20$ and $t \in [0, 50]$, which then lead to $\Delta < 1$ values.

In a two-state model, the entangled quantum states are written as:

$$\Phi(\mathbf{q}; x) = C_1(x)\, \psi_1(\mathbf{q}) + C_2(x)\, \psi_2(\mathbf{q}), \tag{10}$$

where the absolute values of the amplitudes in the two "diabatic" superposition states are [21]:

$$|C_2(x)| = \{1 + (\mathrm{V}_{12}/[E_{full}(x) - U_1(x)])^2\}^{-1/2}, \quad |C_1|^2 + |C_2|^2 = 1, \tag{11}$$

in terms of the 2×2 Hamiltonian matrix elements:

$$\langle \psi_1 | \hat{H}_{full}\, \psi_2 \rangle_{\mathbf{q}} = \langle \psi_1 | \hat{V}_{field} \psi_2 \rangle_{\mathbf{q}} = V_{12}, \tag{12a}$$

$$\langle \psi_i | \hat{H}_{full}\, \psi_i \rangle_{\mathbf{q}} = \langle \psi_i | \hat{H}_e \psi_i \rangle_{\mathbf{q}} = U_i(x), \tag{12b}$$

and the total energy in the field (cf. Eq. 5):

$$E_{full}(x) = U_1(x) + \frac{1}{2}\left\{ \Delta U_{12}(x) - |\Delta U_{12}(x)| \sqrt{1 + 4\left(\frac{V_{12}}{\Delta U_{12}}\right)^2} \right\}, \tag{13}$$

with $\Delta U_{12}(x) = U_2(x) - U_1(x)$. For a simpler notation, we omit all reference to the applied **A**-vector field in the labelling for the total energy $E_{full}(x)$ and the $\{C_i\}$-coefficients.

Once the semiclassical $\{U_i\}$ potentials have been chosen in (7), the results will depend on the choice of coupling element V_{12} in Eq. (12a). In previous works, we have considered a uniform V_{12} value (i.e., independent of the x coordinate) [13,21]. From now on, we refer to this condition as the "*strong global coupling*" (SGC), denoted as $V_{12} = \delta\ f_{\mathrm{SGC}}$, with $f_{\mathrm{SGC}} = 1$. In contrast, an x-dependent V_{12} matrix element is referred to as a *local coupling*, a case that reflects the shape of the external field pulse via a spatially variable **A**-vector. Motivated by the lorentzian-shaped pulses, we have considered the following two choices for local coupling:

$$V_{12} = \delta\ f_{\mathrm{WLC}}, \quad \text{with} \quad f_{\mathrm{WLC}} = \frac{x^2}{1+x^2}, \tag{14a}$$

$$V_{12} = \delta\ f_{\mathrm{SLC}}, \quad \text{with} \quad f_{\mathrm{SLC}} = \frac{1}{1+x^2}, \tag{14b}$$

where "WLC" and "SLC" stand for *weak-local* and *strong-local* coupling, respectively. As the term suggest, the f_{SLC} function magnifies the coupling between the diabatic basis functions around the location of the molecular U_1-attractor. This is the typical situation that would be found when using an STM-tip as the source of the electric field, and placing it exactly at $x = 0$. The weak-field coupling, in contrast, describes the complementary case, i.e., a coupling between diabatic basis functions that is minimal at $x = 0$. Such a situation would be found when lowering the electric field intensity by using a capacitor with an "indentation" at $x = 0$.

The following section discusses how the geometrical properties of the $E_{full}(x)$ function are affected by using these spatially variable local couplings. For simplicity, we focus on Eq. (14), which allow us to maximize and minimize such couplings in the region around $x = 0$. The approach can, of course, be easily generalized to consider other different placements.

3 Phase diagrams for the topology of the total energy function E_{full}

We focus on how the external field affects the occurrence of an effective reaction barrier in E_{full}. Given that we deal presently with a one-dimensional (1D) curve, we adopt a critical-point topology approach [23]; in this context, the $E_{full}(x)$ function can be labelled by the pair $(n_{\mathrm{m}}, n_{\mathrm{M}})$, where n_{m} and n_{M} stands by the number of minima and maxima, respectively, including those associated with the asymptotic limit $x \to +\infty$ for fragmental dissociation.

Even when using 1D-functions, local couplings can give rise to situations with numerous minima and barriers. For simplicity, we focus here on two "phases" in the 2D $(k^{1/2}, \Delta)$-parameter space, namely, a "barrierless phase," and a phase where the effective energy in the field has at least one barrier (the "barriers' phase"). In terms of critical-point topology, the former case corresponds to $(n_{\mathrm{m}}, n_{\mathrm{M}}) = (1, 1)$, with a single maximum at $x \to +\infty$, and the single minimum at a molecular bound state permanently trapped in the field. In contrast, the "barriers' phase" in $E_{full}(x)$ corresponds to two-parameter models that yield $n_{\mathrm{m}} > 1, n_{\mathrm{M}} \geq 1$.

3.1 Illustrative examples

We begin by considering some examples which highlight typical effects caused by the modulation of the external-field couplings introduced in Sect. 2. Figure 1 shows the resulting total energy function E_{full} (*top*), the shape of the local V_{12} coupling (*top inset*), as well as the absolute values of the diabatic $|C_1|$ and $|C_2|$ amplitudes (*bottom*), resulting from the two different couplings. (Since we are not presently concerned with the phases in the diabatic basis states, we refer to $|C_1|$ and $|C_2|$ simply as the "amplitudes"). This figure contrasts the global strong coupling $V_{12} = 50$ and the weak-local coupling $V_{12} = 50 f_{\mathrm{WLC}}$ for a two-state model with $k = 100$ and $t = 50$ in Eq. (7). These values give rise to a diabatic crossing at $x_+ \approx 1.00364$ and a value $\Delta \approx 0.367$ for the diabatic "pseudo-barrier."

As shown by the amplitudes, the WLC yields a superposition state that is more strongly dominated by the "reactant" basis function at $x = 0$ (as a result of V_{12} having

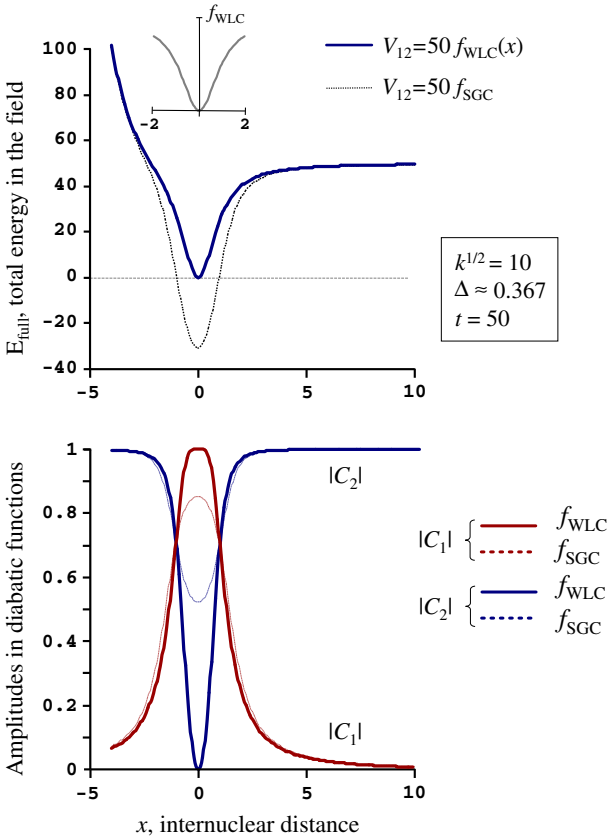

Fig. 1 Effect of a weak-local coupling (WLC) with the external field in a two-state model for bond breaking. The *top* diagram shows the effect on the total energy E_{full}; the *bottom* diagram shows the change in the amplitudes for the coherent superposition (entangled state) between two diabatic basis functions. The "molecular" diabatic basis state corresponds to a harmonic attractor with semiclassical potential energy U_1 with a dimensionless frequency $k^{1/2} = 10$. The "fragmental" diabatic state corresponds to an exponential potential energy with asymptotic limit $U_2(x \to \infty) = 50$, where x is the dimensionless elongation coordinate. The diabatic crossing between two semiclassical potentials produces a pseudo-barrier to bond formation $\Delta \approx 0.364$. In presence of the external field, there is no barrier with a constant strong-global coupling (SGC) with $V_{12} = 50$, nor with a WLC with $V_{12} = 50x^2/(1 + x^2)$. In the latter case, however, the confinement in the field is much less marked. (See text regarding the use of the term "amplitude" in the context of the $\{C_i(x)\}$-coefficients)

a minimum at $x = 0$). Consistently, the WLC produces a less deep single-minimum in E_{full}. In other words, for this particular model, a WLC does not change the E_{full}-topology, but leads to a weaker confinement of the molecular bound state in the field.

The situation can be quite different as we change the $(k^{1/2}, \Delta)$-values. Figure 2 shows the E_{full}-curve and $\{|C_i|\}$-amplitudes for a model with a lower harmonic frequency in U_1 and a lower asymptotic limit for U_2. The parameters used, $k = 25$ and $t = 0$, produce a diabatic crossing at $x_+ \approx 0.2497$ and a pseudo-barrier at $\Delta \approx 0.779$. In this case, the WLC changes the E_{full}-curve radically. As in Fig. 1, the WLC enhances

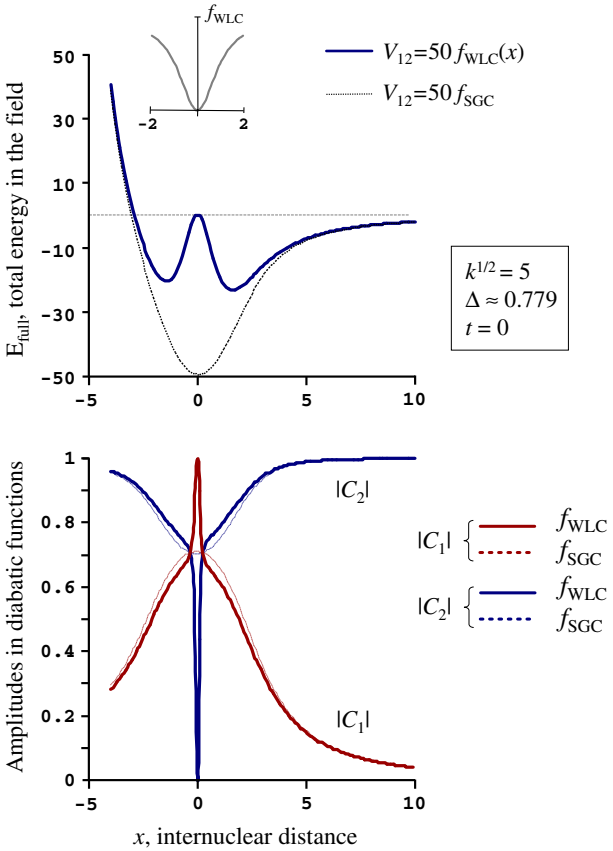

Fig. 2 Effect of a weak-local coupling (WLC) on a two-state model for bond breaking with diabatic pseudo-barrier $\Delta \approx 0.779$ (cf. Fig. 1 for the notation used). The *top* diagram shows how the single-well in a SGC becomes a two-well trap when using a WLC. The f_{WLC}-function effectively raises the energy to that of the harmonic well U_1, thus splitting the E_{full}-well derived with f_{SGC}. The main observable effect in the amplitudes is a sharp $|C_1|$-peak in the "molecular" diabatic function. As in Fig. 1, these behaviours are the direct result of the WLC enhancing the $|C_1|$-amplitude at $x = 0$

the dominance of the amplitude at $|\psi_1\rangle$ around $x = 0$ in the quantum state. However, the $|C_1|$-peak is much sharper in this case, which results in an asymmetric double-well for E_{full}, with a barrier centred at $x = 0$. In this case, the SGC model produces a deep attractor with the same topology as in Fig. 1, i.e., $(n_{\mathrm{m}}, n_{\mathrm{M}}) = (1, 1)$, while the weak coupling changes that topology to $(n_{\mathrm{m}}, n_{\mathrm{M}}) = (2, 2)$.

Figure 3 shows how the behaviour in Fig. 2 changes if the asymptotic dissociation limit is raised to $t = 50$ (cf. Eq. 7b), thereby lowering the diabatic pseudo-barrier to $\Delta \approx 0.132$. In this case, the WLC broadens the $|C_1|$-peak around $x = 0$, which in turns leads to a *very shallow triple-well* in the E_{full}-function. In other words, while the SGC model with $V_{12} = 50$ still produces a single-well E_{full}-curve for this model, the WLC model changes its topology from $(n_{\mathrm{m}}, n_{\mathrm{M}}) = (1, 1)$ to $(n_{\mathrm{m}}, n_{\mathrm{M}}) = (3, 3)$.

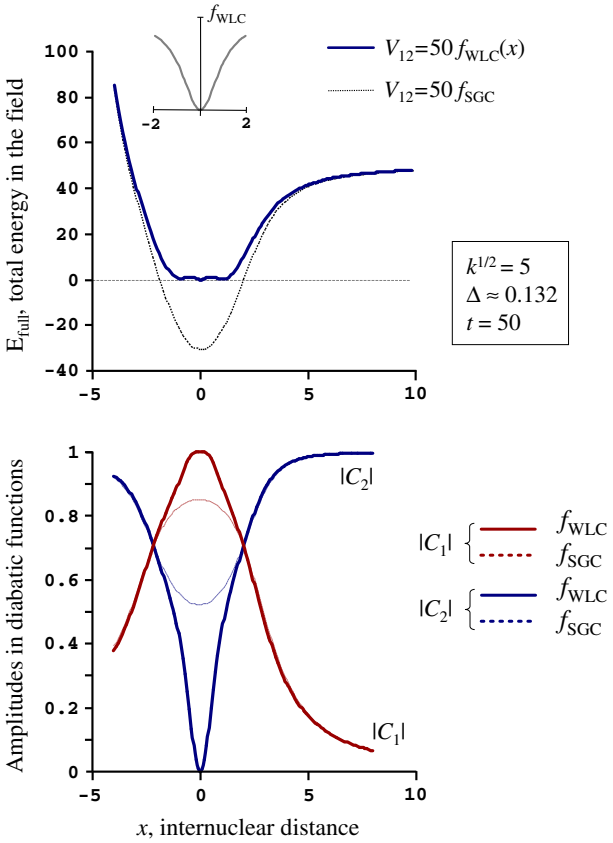

Fig. 3 Effect of a WLC on a two-state model for bond breaking with a small semiclassical diabatic pseudo-barrier, $\Delta \approx 0.132$ (cf. Fig. 1 for the notation used). In this case, the WLC transforms the single-well attractor obtained with the SGC into a rather flat well with three very shallow minima. As in Figs. 1 and 2, the WLC induces a larger $|C_1|$-amplitude near $x = 0$

Finally, Fig. 4 shows the different effects associated with a *strong*-local coupling (here, using $V_{12} = 15\,f_{SLC}$). The model in Fig. 4 can be contrasted with that in Fig. 2. In this case, we have considered a weaker harmonic frequency ($k = 1$), which lowers the pseudo-barrier to $\Delta \approx 0.406$, but the overall effect of the uniform coupling $V_{12} = \text{const}$ is similar in Figs. 2 and 4, i.e., both generate a broad single-well in E_{full}. However, while the introduction of a WLC leads to a double-well in Fig. 2, the use of a lorentzian-shaped SLC in Fig. 4 maintains the single-well topology. Nevertheless, the E_{full}-well is qualitatively changed by the nonuniform coupling $V_{12} = 15\,f_{SLC}$. Note that the strong coupling switches much more rapidly the $|C_i|$-amplitudes, particularly for $x > x_+ \approx 0.901$ (Fig. 4, bottom), thereby producing quantum states whose wave functions resemble locally the diabatic basis states more strongly than when using the SGC. As a result, the E_{full}-well with the local field is more harmonic. While the SGC shifts the minimum in E_{full} to $x > 0$ and produces a strong asymmetry around $x = 0$, the total energy curve with a SLC is essentially a harmonic well centred at $x = 0$ for

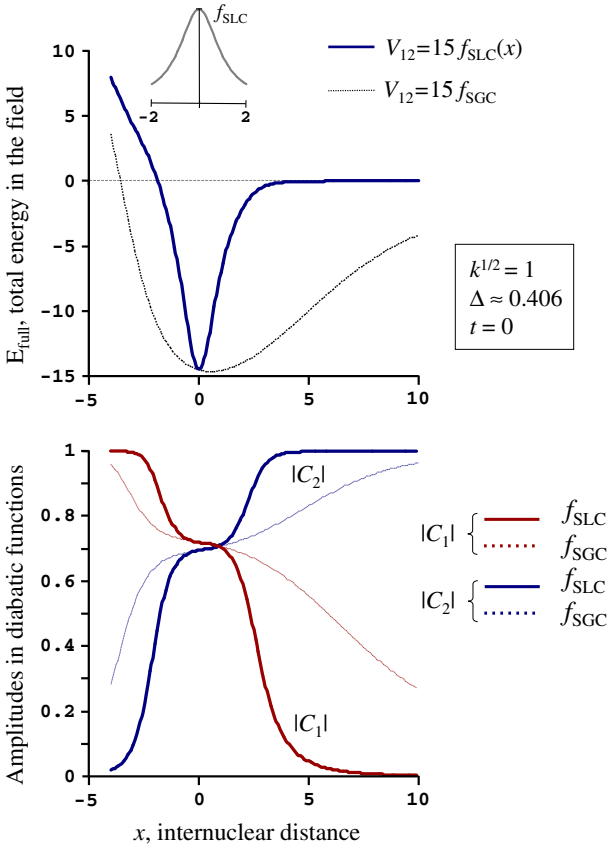

Fig. 4 Effect of a strong-local coupling (SLC) on the same two-state model for bond breaking/formation used in Figs. 1, 2 and 3. In this case, the distance-dependent coupling $V_{12} = 15 f_{\mathrm{SLC}}(x)$ leads to a rapid switch in $|C_i|$-amplitudes, as opposed to the gradual change observed when using the SGC with $V_{12} = 15$. As a result, the total energy $E_{full}(x)$ changes quickly into the asymptotic "product" energy U_2-channel. The overall effect is a single-well attractor that is much confining and harmonic that the one produced in the presence of a strong-global coupling. The latter case (*dotted line*) produces a wider anharmonic well, with a clear shift to larger equilibrium bond lengths

$E_{full} < -5$. While the stretching (or "softening") of a bond by a laser field has been discussed in the literature [24], our results predict that this effect could be switched off by modifying the geometry of the applied field.

3.2 Phase diagrams

The four examples in Sect. 3.1 illustrate some of the typical behaviours encountered within the continuum of two-state models defined over the range of $(k^{1/2}, \Delta)$-values. We can now discuss the general trends by classifying the $(k^{1/2}, \Delta)$-parameter space in terms of two different topological phases, namely, the models leading to "barrierless" E_{full} curves, and those leading to curves with at least one barrier (the "barriers' phase").

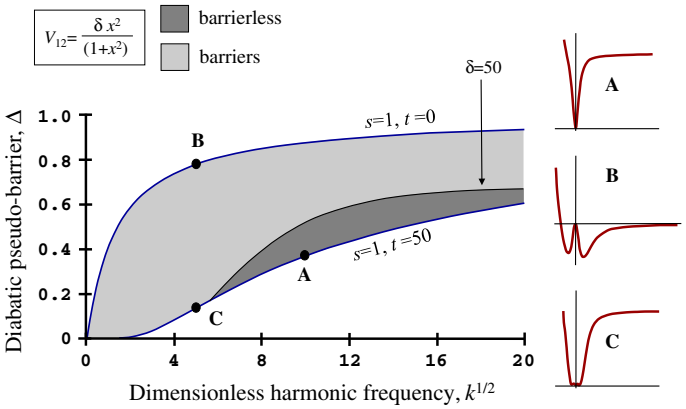

Fig. 5 Phase diagram for the critical-point topologies of E_{full} in parameter space for two-state models of bond breaking/formation, in presence of a weak-local coupling with the external field, $V_{12} = \delta\ f_{\mathrm{WLC}}(x)$. The shaded areas correspond to solutions in the $(k^{1/2}, \Delta)$-pairs for $s = 0$ and $t \in [0, 50]$ in Eq. (8). The *dark shading* defines the collection of two-state models that produce a single attractor in E_{full} with $\delta = 50$ (i.e., the "barrierless phase" denoted by the *inset* point *A*). The *light shading* corresponds to "barriers' phase" (i.e., topologies with barriers), as illustrated with the *insets B* and *C*. The chosen points *A*, *B*, and *C* correspond to the cases depicted in Figs. 1, 2, and 3, respectively

Figure 5 shows the phase diagram associated with the quantum states with a weak-local coupling $V_{12} = 50 f_{\mathrm{WLC}}$. In this case, the "barrierless phase," indicated with the darker shading, only emerges for models with $k^{1/2} > 6$ and pseudo-barriers with $\Delta < 0.7$. The three highlighted points A, B, C correspond respectively to the models illustrated in Figs. 1, 2, and 3. The cases B and C belong to the "barriers' phase," although the near vicinity of point C to the frontier of the "barrierless phase" conveys clearly the fact that the barriers are very shallow in the latter model.

Figure 6 displays the shift in the phases as one changes the δ-value, i.e., the intensity of the weak-local coupling as defined by *max* (V_{12}). (For clarity, we only display the frontiers between the two phases, in dashed lines). As in Fig. 5, the "barrierless phase" is always found *under* the denoted frontier curves. It is clear that, while maintaining the f_{WLC}-function, the intensity of the external field changes dramatically which $(k^{1/2}, \Delta)$-values lead to barrier-free E_{full}-curves. The following observations can be made following Figs. 5 and 6:

(a) The "barrierless phase" appears in low-frequency harmonic molecular diabatic states (e.g., $k^{1/2} < 4$) when the intensity of the external field coupling is as low as $\delta = 1$. For such low δ-values, however, the frontier of the phase falls sharply as the k-value increases.
(b) The "barrierless phase" initially grows in extension with δ, when measured as an area in $(k^{1/2},\ \Delta)$-parameter space, but then decreases again as the δ-value becomes too large.
(c) Eventually, within any given range of k and t values (cf. Eq. 7), all two-state models lead to quantum states with multi-minima E_{full}-wells for sufficiently large δ-values. In other words, as the external field increases, the weak local coupling

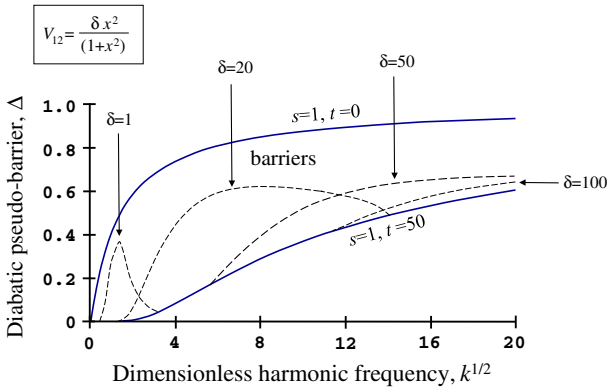

Fig. 6 Shift in the boundary of the "barrierless phase" as the intensity of the WLC with the external field increases (i.e., larger δ-values). The "barrierless phase" in ($k^{1/2}$, Δ)-space corresponds to areas *below* the *dashed-line* curves. Note that a sufficiently large V_{12}-coupling leads eventually to a predominance of E_{full}-solutions *with* barriers

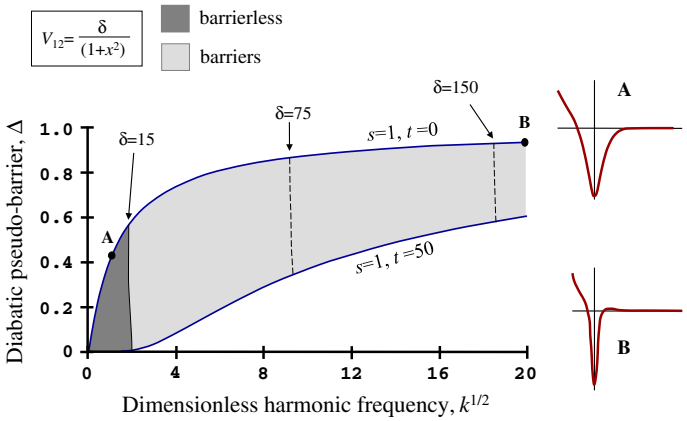

Fig. 7 Shift in the boundary of the "barrierless phase" as the intensity of the SLC with the external field increases (i.e., larger δ-values). The "barrierless phase" in ($k^{1/2}$, Δ)-space is always to the *left* of the regions delimited by the *dashed-lines*. The *insets A* and *B* correspond, respectively, to the case $\delta = 15$, where they are associated with a non-barrier case (*A*) and with a small barrier (*B*). The detailed behaviour for points *A* and *B* are shown in Figs. 4 and 8, respectively

makes it very unlikely that the entangled quantum state will be fully confined within a single-well E_{full}-function.

A very different situation emerges when using SLC representation. Figure 7 shows the phase diagram in the same ($k^{1/2}$, Δ)-parameter space as in Figs. 5 and 6, but this time for the SLC function $V_{12} = \delta\ f_{\mathrm{SLC}}$. When using $\delta = 15$, as in Fig. 4, the "barrierless phase" occupies a small sliver of parameter space with $k^{1/2} < 2$ (dark shading). The two insets on the right-hand side highlight the two different topologies as follows: (*i*) the barrierless curve for point A corresponds exactly to the case illustrated in Fig. 4; (*ii*) point B exhibits a very small, yet nonzero, dissociation barrier for $x > 0$.

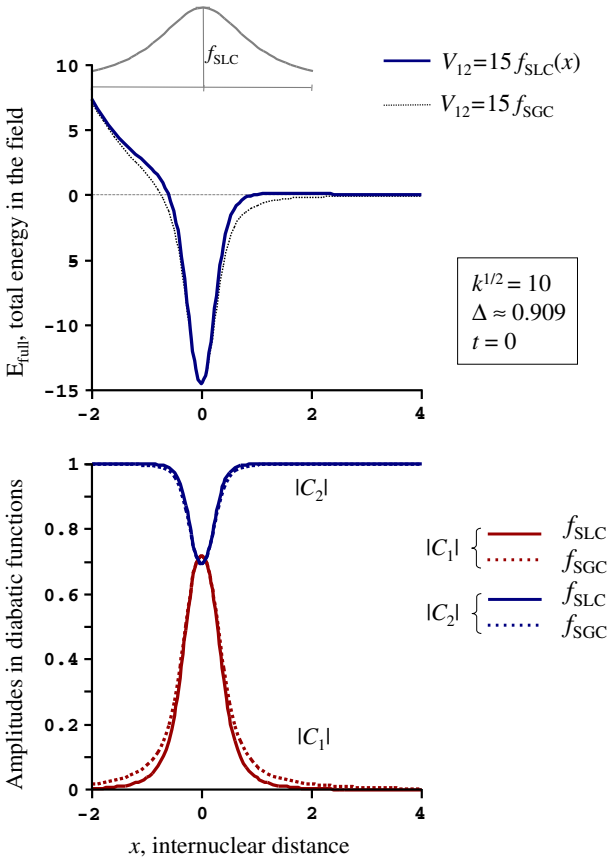

Fig. 8 Total energy and superposition amplitudes for the point *B* in Fig. 7. This case corresponds to a strong-local coupling to the external field for a two-state model with a large barrier and a highly confining harmonic potential U_1. For illustration, the profile of the V_{12}-coupling is depicted over the *top* diagram, at the same scale of x-values. Note that the effect of the strong-local coupling is a subtle narrowing of the well's width which leads to the occurrence of a small barrier for bond breaking

The detailed behaviour for point B is displayed in Fig. 8, and contrasted with the strong-global coupling case of $V_{12} = 15$. Note that, although the effect is very small in the $\{|C_i|\}$-amplitudes, the global coupling broadens sufficiently the E_{full}-well obtained in the SLC model (for $E_{full} > -5$) so as to eliminate the corresponding energy barrier.

As δ increases, the frontier between the two phases is displaced almost horizontally to the right, leading to a phase diagram that becomes dominated by the "barrierless phase." In other words, the SLC behaves exactly opposite to the WLC in Figs. 5 and 6: as the field intensity increases, the entangled quantum states become confined in a deeper single-well. These predicted behaviours could be tested experimentally by monotoring how the rate and energetics of simple bond breaking processes change when exposed to field-pulse setups with distinct geometries.

4 Conclusions

In the present quantum methodology, the process of bond breaking (or formation) is described as a field-modulated change in amplitude in coherent quantum states over laboratory space, i.e., akin to electronic transitions. In the presence of the external field, the quantum system is able to evolve in such a way so as to open a large amplitude in a particular "product" reaction channel. The information about that possible "exit" channel is already incorporated in the initial entangled state; contrary to the standard electronuclear approaches [25], the breaking of a bond does not result from an increasing separation between nuclei, but rather by the manner in which the external field couples the components of the superposition state [13], namely, the molecular bound (or "reactant") state and the asymptotically separated fragment (or "product") state. The present approach emphasizes the quantum nature of a bond breaking or formation processes: the external field essentially brings the bound and unbound entangled states into a superposition where they coexist in a continuum resembling a Feshbach resonance [26]. This resonance allows the chemical process to flow back and forth in an equilibrium [15], until decoherence (e.g., via photon emission or collision with another body) forces the system to cool down into a reactant or product state.

The present results show that the external field can be used as a fine tuning tool, in addition to its generic role as a catalyst for the actual chemical process. By modifying not only the intensity, but also the symmetry and geometry of the applied electric vector potential, one could, in principle, manipulate the topology of the total energy for the quantum states dressed in the field. Depending on our choice of external field couplings, it is possible to confine a quantum state at a dominant configuration in laboratory space, or to produce several trapping configurations separated by effective barriers. Further control can also be introduced by varying location of the maxima and minima of the coupling matrix elements. In a future work, we shall explore this possibility for more complex reactions that require diabatic schemes based on multistate models.

Acknowledgments Gustavo A. Arteca acknowledges support by NSERC (Canada) and the continued hospitality of the Department of Physical and Analytical Chemistry (Uppsala, Sweden).

References

1. R.V. Krems, Int. Rev. Phys. Chem. **24**, 99 (2005)
2. R.V. Krems, A. Dalgarno, Phys. Rev. A **68**, 013406 (2003)
3. S. Cornish, Physics **1**, 24 (2008)
4. R. Côté, Nat. Phys. **2**, 583 (2006)
5. Y. Xia, L. Deng, J. Yin, Appl. Phys. B **81**, 459 (2005)
6. A. Giusti-Suzor, F.H. Mies, L.F. Di Mauro, E. Charron, B. Yang, J. Phys. B **28**, 309 (1995)
7. A.D. Bandrauk, E.-W.S. Sedik, C.F. Matta, Mol. Phys. **104**, 95 (2006)
8. P. Král, I. Thanapoulos, M. Shapiro, Rev. Mod. Phys. **79**, 53 (2007)
9. J.I. Cirac, P. Zoller, Phys. Today **57**, 38 (2003)
10. D. DeMille, Phys. Rev. Lett. **88**, 067901 (2002)
11. A. André, D, DeMille, J.M. Doyle, M.D. Lukin, S.E. Maxwell, P. Rabl, R.J. Schoelkopf, P. Zoller, Nat. Phys. **22**, 636 (2006).
12. G.A. Arteca, O. Tapia, Phys. Rev. A **84**, 012115 (2011)

13. G.A. Arteca, J.M. Aulló, O. Tapia, J. Math. Chem. **50**, 949 (2012)
14. O. Tapia, Adv. Quantum Chem. **56**, 31 (2009)
15. O. Tapia, Adv. Quantum Chem. **61**, 49 (2011)
16. R. Crespo, M.-C. Piqueras, J.M. Aulló, O. Tapia, Int. J. Quantum Chem. **111**, 263 (2011)
17. G.A. Arteca, O. Tapia, Int. J. Quantum Chem. **107**, 382 (2007)
18. G.A. Arteca, J.P. Rank, O. Tapia, J. Theor. Comp. Chem. **6**, 869 (2007)
19. G.A. Arteca, J.P. Rank, O. Tapia, Int. J. Quantum Chem. **108**, 651 (2008)
20. G.A. Arteca, J.P. Rank, O. Tapia, Int. J. Quantum Chem. **108**, 1810 (2008)
21. G.A. Arteca, O. Tapia, J. Math. Chem. **35**, 1 (2004)
22. G.A. Arteca, O. Tapia, J. Math. Chem. **35**, 159 (2004)
23. P.G. Mezey, *Potential Energy Hypersurfaces* (Elsevier, Amsterdam, 1987)
24. A. Hishikawa, A. Iwamae, K. Yamanouchi, Phys. Rev. Lett. **83**, 1127 (1999)
25. L.J. Butler, Annu. Rev. Phys. Chem. **49**, 125 (1998)
26. H. Feshbach, Ann. Phys. **5**, 357 (1958)